

See discussions, stats, and author profiles for this publication at: <https://www.researchgate.net/publication/231661554>

Dual-Level Direct Dynamics Calculations of Deuterium and Carbon-13 Kinetic Isotope Effects for the Reaction Cl + CH₄

ARTICLE *in* THE JOURNAL OF PHYSICAL CHEMISTRY A · MAY 1998

Impact Factor: 2.69 · DOI: 10.1021/jp980759l

CITATIONS

56

READS

33

3 AUTHORS:



Orlando Roberto Neto

Instituto de Estudos Avançados

2 PUBLICATIONS 56 CITATIONS

[SEE PROFILE](#)



Elena Laura Coitiño

University of the Republic, Uruguay

45 PUBLICATIONS 700 CITATIONS

[SEE PROFILE](#)



Donald Truhlar

University of Minnesota Twin Cities

1,342 PUBLICATIONS 81,158 CITATIONS

[SEE PROFILE](#)

University of Minnesota Supercomputing Institute Research Report UMSI 98/54

UMSI 98/54 March 1998

**DUAL-LEVEL DIRECT DYNAMICS
CALCULATIONS OF DEUTERIUM AND
CARBON-13 KINETIC ISOTOPE EFFECTS
FOR THE REACTION Cl + CH₄**

Orlando Roberto-Neto, Elena L. Coitiño,
and D.G. Truhlar

1200 Washington Avenue South □ Minneapolis, Minnesota 55415

January 8, 1998
with minor revisions March 20, 1998
submitted to *J. Phys. Chem. A*

**Dual-Level Direct Dynamics Calculations of Deuterium and
Carbon-13 Kinetic Isotope Effects for the Reaction Cl + CH₄**

Orlando Roberto-Neto[†], Elena L. Coitiño[‡] and D. G. Truhlar*

Department of Chemistry and Supercomputer Institute

University of Minnesota

Minneapolis, Minnesota, 55455-0431

[†]Permanent address: Instituto de Estudos Avançados, Centro Técnico-Aeroespacial,
Rodovia dos Tamoios km 5,5, São José dos Campos (SP), CEP 12231-970, Brasil
orlando@ieav.cta.br

[‡]Permanent address: Laboratorio de Química Teórica y Computacional, Facultad de
Ciencias, Tristan Narvaja 1674, cc 10773, Montevideo, Uruguay, laura@fcien.edu.uy

*Corresponding author

ABSTRACT

The kinetic isotope effects, KIEs, for hydrogen abstraction from the isotopomers CH_4 , $^{13}\text{CH}_4$, CH_3D , and CD_4 by chlorine atoms have been studied by the dual-level direct dynamics approach with the MORATE computer program. Low-level calculations of the potential energy surface were carried out at the NDDO-SRP level (in particular the AM1-SRP level), using two different sets of specific reaction parameters labeled SRP4 and SRP13. High-level structural and energetic properties of the reactants, saddle point, and products were obtained at the MP2-SAC and MP2 levels using the 6-311G(2d,d,p) basis set and were used to interpolate corrections to the low-level calculations. The dual-level calculations were carried out using the ICL-Eckart improved interpolated corrections algorithm. Tunneling was included by the microcanonical optimized multidimensional tunneling (μOMT) method, and we find that large-curvature tunneling paths usually provide the dominant contribution, with significant participation of excited vibrational states. Both rectilinear and curvilinear coordinates were applied to the unsubstituted reaction. The $^{12}\text{C}/^{13}\text{C}$ KIEs calculated at the MP2-SAC//SRP4 level using MP2 frequencies are in very close agreement with the experimental ones, with values of 1.07 and 1.06 at 243 and 297 K, respectively, as compared to experimental values of 1.07 at both temperatures. For the reaction $\text{CH}_3\text{D} + \text{Cl}$, the calculated H/D KIEs are equal to 1.55 and 1.45 at 223 and 296 K while the measured values are equal to 1.59 and 1.50, respectively. The H/D KIE for the reaction $\text{CD}_4 + \text{Cl}$ is calculated to decrease from 11 to 4.7 as the temperature increases from 300 K to 450 K, whereas the experimental value decreases from 12 to 3.9. We also make comparison with previous results for the reaction unsubstituted $\text{CH}_4 + \text{Cl}$.

1. INTRODUCTION

The last few years have witnessed great concern about changes in the chemical composition of the Earth's atmosphere, and a significant amount of research has been devoted to this question. One of the principal subjects of the recent studies is methane.^{1,2} Methane is an important greenhouse gas whose relative concentration in the stratosphere and troposphere is affected by reaction with the radicals OH(² Π), O(¹D), and Cl(²P). A very useful indicator of the sources and sinks of methane in the environment is provided by measurements of the ¹²/¹³CH₄ ratios,^{1,2} and interpretation of these data requires an understanding of the kinetic isotope effects (KIEs) of several processes that lead to fractionation. Until recently the reaction of CH₄ with OH, which has a ¹²/¹³C KIE equal to 1.005 ± 0.001 ,^{3a} was considered the main sink process for CH₄, but recent atmospheric measurements of the ¹²/¹³CH₄ ratios showing a higher fractionation of approximately 1.012 are not in agreement with an exclusive OH contribution. In fact the atmospheric chemistry of methane seems to be better modeled in terms of a CH₄ + Cl sink by using the experimental KIE of 1.066 ± 0.002 measured^{3b} in the laboratory at T = 297 K. A second reason why the Cl + CH₄ reaction is atmospherically important is that it converts Cl, an active ozone destroyer, into inactive HCl.

Another KIE of the Cl + CH₄ reaction that has important atmospheric implications is the ratio of the rate of reaction of Cl with CH₃D⁴⁻⁶ to the rate of reaction of Cl with CH₄. Approximately 99% of the partially deuterated methane in the atmosphere is in the form of CH₃D, and recent and accurate measurements using tunable diode laser spectroscopy⁵ yield values for the H/D KIEs decreasing from 1.59 to 1.51 as the temperature increases from 223 K to 296 K. Another important H/D KIE is that for the reaction between Cl and CD₄ which is not so well studied^{6,7} experimentally and has a value of the H/D KIE equal to 12.2 ± 0.9 at room temperature.⁶

We have recently studied the kinetic isotope effect for several reactions including ¹³CH₄ + OH and CD₄ + OH,⁸ using conventional and variational transition state theories

(TST and VTST) with tunneling included by multidimensional semiclassical methods. Previous theoretical work on the Cl + CH₄ KIEs is sparse.⁹ For the ¹²C/¹³C KIE, Tanaka et al.^{9a} combined electronic structure calculations at the MP2/6-311G(3d,2p) level with conventional TST including Wigner and Eckart tunneling corrections; they found, for instance, a ¹²C/¹³C KIE of 1.026 at 300 K and a small temperature dependence. (MP2 denotes Møller-Plesset second-order perturbation theory based on a Hartee-Fock reference wave function.) On the other hand, experimental measurements show values of this KIE varying from 1.075 to 1.066 as the temperature varies from 223 to 297 K.^{3b} Chen et al.^{9b} calculated the KIE for CD₃ + DCl → CD₄ + Cl, and this can in principle be combined with the equilibrium isotope effect to yield a prediction for the Cl + CD₄ KIE. However, they did not provide their calculated value of the equilibrium isotope effect.

In addition to studying KIEs, we will calculate absolute rate constants and compare them to several other theoretical studies^{10–15} of ¹²CH₄ + Cl and its reverse. In earlier work in our group, the geometry and the frequencies of the transition state were calculated with the MP2-SAC method with a 6-311G(2d,d,p) basis set.¹⁰ (Note: 6-311G and MC-311G are identical for the systems considered here, and the reader should not be confused that we used the latter notation in Ref. 10. Note also that SAC denotes scaling all correlation energy.) This calculation yielded a classical barrier height of 7.9 kcal/mol and a zero-point-inclusive barrier height (evaluated at the saddle point) of 4.8 kcal/mol. In a later study in our group, Gonzalez-Lafont et al.¹¹ used the same level of electronic structure calculations to calculate rate constants at the dynamical level of canonical variational theory (CVT) with small-curvature tunneling (SCT). The calculations were carried out by second-order interpolated variational transition state theory with permutation of vibrational frequencies to align them for the most accurate possible interpolation (IVTST-2P). The published rate constants agree with experiment within a factor of about 2 over the whole 200–500 K temperature range.

In the present study, a new version,¹⁶ denoted ICL-Eckart, of the VTST-with-interpo-

lated-corrections (VTST-IC) scheme, for carrying out dual-level direct dynamics^{17–19} is used to calculate thermal rate constants and KIEs for the reactions of Cl with CH₄, ¹³CH₄, CH₃D, and CD₄. Potential energy surfaces (PESs) are obtained using AM1-SRP semiempirical methods for the low level, and ab initio MP2-SAC/6-311G(2d,d,p) calculations are used for the high level to interpolate corrections to low-level values of energetic quantities, vibrational frequencies, and moments of inertia. (AM1-SRP denotes a combination of AM1 general parameters and specific reaction parameters (SRP) in a neglect-of-diatom-overlap (NDDO) semiempirical molecular orbital wave function; AM1 denotes Austin model 1.) Using the dual-level implicit PES, VTST calculations including microcanonical optimized multidimensional tunneling (μ OMT) are used to calculate the forward and reverse reaction rates and the KIEs. The μ OMT calculations are optimized at each energy rather than just for the thermal average, and they allow for small and wide corner cutting and the direct participation of excited vibrational motions in the tunneling dynamics.

In section 2 we summarize the methods used in this work. Section 3 contains our results and makes comparison to previous work.

2. METHODS

2.1 Eletronic Structure Calculations

In dual-level direct dynamics, we use low-level (LL) or low-cost calculations to construct energies, gradients, and hessians, as needed, of the complete potential energy surface. Then a high level (HL) method is applied in calculations on the critical elements of the surface, in particular to obtain stationary-point geometries, frequencies, and energies which are used to interpolate corrections to the LL potential energy surface, both in the valley along the reaction path and also in the corner cutting swath traversed by the system during large-curvature tunneling.

In the present study the high level is the MP2-SAC/6-311G(2d,d,p) approach presented previously.¹⁰ In this method, we use the triple split 6-311G²⁰ basis set with polarization functions having exponential parameters $\alpha_p = 0.75$ for the hydrogen, $\alpha_d = 0.626$

for the carbon, and $\alpha_d = 1.04$ and 0.34 for the chlorine atom. Six Cartesian functions were used in the d sets. Correlation energy is included for both core and valence-shell electrons at the MP2 level. For the scaling factor of the SAC method,^{10,21} a value of $F = 0.835$ is used; this is the average of the values of 0.84 determined from the H-Cl bond dissociation energy and 0.83 determined¹⁰ from the H-C bond dissociation energy with the chosen basis set. A main goal of the MP n -SAC^{10,21} method is to make the theoretical energy difference between reactants and products match closely with the experimental one, so as to achieve a balanced treatment for the forward and reverse rate constants. Theoretical treatments that yield the correct energy of reaction are more likely to predict qualitatively correct transition state geometries. We shall compare the calculated and experimental energies of reaction in Section 3.2.

For the low-level surface, calculations were performed using the SRP approach.^{22,23} The philosophy of this method is that we can achieve better results for energetics and structural and dynamical properties for a specific reaction by using modified (system-specific) NDDO parameters adjusted with the help of experimental exoergicities, activation energies, or rate constants or by using ab initio calculations. The modified parameters are called specific reaction parameters (SRP). It is important in the VTST-IC method that the low-level method generates reasonably accurate values for the structural quantities, especially the stationary-point geometries but also the geometries along the rest of the reaction path. In adjusting the parameters of the AM1 method to achieve this goal for the Cl + CH₄ reaction, four NDDO parameters were optimized²³ by a genetic algorithm to achieve as good as possible agreement with MP2/cc-pVDZ calculations at either 4 or 13 geometries along the reaction path, in both cases including the reactants, products, and saddle point. The resulting sets of AM1-SRP parameters are called²³ SRP4 and SRP13, respectively, in the rest of this paper. The present study is the first time that these sets of parameters have been used in variational transition state calculations.

The full potential energy surface (PES) was constructed first at the AM1-SRP level

and then “corrected” by an interpolation algorithm described previously;^{17,19} the use of two levels in this way is called VTST-IC (VTST with interpolated corrections) or dual-level direct dynamics. Values of the classical barriers height, harmonic vibrational frequencies, and determinants of the moment of inertia tensor were calculated from MP2-SAC/6-311G(2d,d,p) calculations of the stationary points, i.e., reactants, products, and saddle point. These MP2-SAC/6-311G(2d,d,p) calculations were used to supply all high-level information needed for the VTST-IC approach. The semi-empirical calculations were done using the MORATE²⁴ code, MORATE is an interface between the MOPAC²⁵ electronic structure package and the POLYRATE²⁶ code. The MP2-SAC calculations were carried out with a locally modified version of the GAUSSIAN 94 code,²⁷ modified to allow geometry optimizations with SAC gradients.

2.2 Dynamics Calculations

The dynamics calculations were carried out using variational transition state theory with interpolated corrections, called VTST-IC or dual-level direct dynamics. The reference path was taken to be the minimum energy path (MEP) obtained by following the steepest descent path of the potential from the saddle point in a mass-weighted or mass-scaled coordinate system scaled to a reduced mass μ ,²⁸

$$x_{i\alpha} = \left(\frac{m_i}{\mu}\right)^{1/2} R_{i\alpha} \quad (1)$$

where m_i is the mass of the atom i , μ is an arbitrary scaling mass which in this work we set equal to 10.992 amu, which equals the reduced for relative translational motion of reactants in the perprotio case, and $R_{i\alpha}$ is a Cartesian coordinate ($\alpha = x, y, \text{ or } z$) of atom i . Geometries along the MEP on either side of the saddle point were calculated using the Euler single-step^{28,29} method with steps of length $0.001 a_0$ (0.0005 \AA). The values of the Hessians and the harmonic vibrational frequencies along the path were calculated at intervals of $0.005 a_0$ (0.0026 \AA). The reaction coordinate s is the signed distance along the MEP through mass-scaled coordinates.

For a canonical ensemble, the variational rate constant for a bimolecular reaction is given by²⁸

$$\begin{aligned} k^{CVT}(T) &= \min k^{GT}(T, s) \\ &= \sigma \tilde{k} T \frac{Q^{GT}(T, s_*^{CVT})}{\Phi^R(T)} e^{-V_{MEP}^{CVT}/\tilde{k} T} \end{aligned} \quad (2)$$

where $k^{GT}(T, s)$ is the rate constant at temperature T for a generalized transition-state (GT or GTS) localized at a value s of the reaction coordinate; s_*^{CVT} is the value of s at which $k^{GT}(T, s)$ has a minimum; σ is the symmetry factor³⁰ which accounts for the reaction path multiplicity (and for the perproto or perdeuterio reaction studied here has values of 4 and 2 for the forward and reverse reaction, respectively); and $\Phi^R(T)$ and $Q^{GT}(T, s_*^{CVT})$ are the reactant and variational transition state partition functions, with the former on a per unit volume basis. The chlorine atom has two low-lying fine structure electronic states, ${}^2P_{1/2}$ and ${}^2P_{3/2}$, with a separation³¹ of $\Delta E = 882 \text{ cm}^{-1}$ due to spin-orbit coupling. It is particularly simple to account for the effect of these states when only the ground electronic state of the transition state is reactive,³² which is an excellent approximation in the present case. In a case such as this the effect of multiple electronic states is simply to multiply the rate constants calculated for the ground electronic state of the transition state by the statistical fraction of collisions that occur on this potential surface. This fraction, called the multiple-surface coefficient, is equal to the electronic degeneracy of the ground state of the transition state divided by the electronic partition function of the reactants. This is the same as the ratio of the electronic partition function of the transition state to the electronic partition function of the reactant under the assumption that there are no low-lying electronically excited states of the transition state. In the present case the ground state of the transition state is a doublet, and the multiple-surface coefficient is given by

$$Q_{elec}^{GT/R} = \frac{2}{4 + 2\exp(-\Delta E/\tilde{k} T)} \quad (3)$$

This factor decreases from 0.4996 at 200 K to 0.4384 at 1000 K and finally to 1/3 in the high-*T* limit.

In principle there is a second effect of the spin-orbit coupling in addition to this statistical coefficient. This is the effect of spin-orbit coupling on the barrier height. The simplest assumption is that spin-orbit coupling is fully quenched at the transition state, as in the F + H₂ reaction.³³ This would raise the barrier by 0.8 kcal (one third of the spin-orbit splitting) as compared to the nonrelativistic Born-Oppenheimer limit. This latter effect is not usually included, and it will not be included here since we do not know the geometry dependence of the remaining spin-orbit effect. Furthermore the effect partly cancels the incompleteness of the one-electron basis set and the treatment of electron correlation, effects that we compensate by the SAC method. In the future, as one uses larger and larger basis sets and more complete treatments of electronic correlation, we will eventually find that this spin-orbit effect is larger than the uncertainty in the correlation energy, and it will be necessary to include it for a complete understanding of the system. In fact, it is interesting to notice that the quenching of the energetic effect of the spin-orbit coupling is probably very general for reactions of Cl and other halogen atoms; it follows mainly from the increase in Σ - II separation at the transition state, a general effect, rather than from any system-specific variation of spin-orbit matrix elements with geometry.

To account for quantum effects on the motion along the reaction coordinate, $k^{CVT}(T)$ is multiplied by a ground-state transmission coefficient³⁴ $\kappa^{CVT/G}$ which accounts for tunneling and nonclassical reflection effects. The quantized rate constant is given by^{28,34}

$$k^{CVT/G}(T) = \kappa^{CVT/G}(T) k^{CVT}(T) \quad (4)$$

Several semi-classical tunneling approximations are used in this present paper to illustrate their effect on the KIE calculations.

The minimum energy path semiclassical adiabatic ground-state (MEPSAG) transmission coefficient is calculated by assuming that the reaction path has negligible curvature

so that the tunneling path essentially coincides with it.^{34,35} The transmission coefficients calculated by this approach are labeled ZCT (zero-curvature tunneling). A more accurate approach, which includes corner cutting on the concave side of the MEP when the reaction-path curvature is small, is the centrifugal-dominant small-curvature semiclassical adiabatic ground-state approximation (CD-SCSAG) or for short SCT (small-curvature tunneling approximation).^{8b,36a} Another method especially designed to treat cases with very large curvature of the reaction path, most commonly encountered in thermoneutral bimolecular or nearly thermoneutral bimolecular reactions with the heavy-light-heavy mass combination, is the large-curvature ground-state approximation, version 3, called LCG3 or LCT. This last approach considers contributions from all straight-line tunneling paths with equal pre- and post-tunneling reaction coordinate components of the kinetic energy, and it also includes tunneling directly into excited vibrational states in the exoergic direction of reaction (and, therefore, by detailed balance, out of excited vibrational states in the endoergic direction).³⁶ Finally an efficient approach well suited to intermediate-curvature cases of tunneling is the microcanonical optimized multidimensional tunneling (μ OMT) approximation.³⁷ In this method, the tunneling probability for each total energy is calculated by both the SCT and LCT approximations, and whichever gives the larger tunneling probability is accepted as the better result; then the results are thermally averaged.

The vibrationally adiabatic ground-state potential curve is given in the harmonic approximation by

$$V_a^G(s) = V_{MEP}(s) + \frac{1}{2}\hbar \sum_{m=1}^{3N-7} \omega_m(s) \quad (5)$$

where $V_{MEP}(s)$ is the electronic potential along s , $\omega_m(s)$ are the generalized normal-mode frequencies at a given s , and the second term accounts for the sum of the zero point vibrational energies (ZPVEs) of all the modes transverse to the reaction path. For most results presented in this paper the generalized normal-mode frequencies along the path are calculated using rectilinear coordinates;²⁸ in selected cases, we also carried out the

calculations using redundant curvilinear coordinates³⁸ and the results are compared. All the VTST-IC reaction rate constants calculations were carried out with MORATE.²⁴

According to our dual-level notation,¹⁹ the calculations with the SRP4 low level are denoted MP2-SAC/6-311G(2d,d,p)///SRP4. In the rest of this paper though, we will use the shorter name SRP4-IC. We also performed calculations in which we used MP2/6-311G-(2d,d,p) frequencies instead of MP2-SAC frequencies. The full name for such a calculation, according to systematic nomenclature,¹⁹ would be MP2-SAC/6-311G(2d,d,p)[MP2/6-311G(2d,d,p)]///SRP4 when SRP4 is the low level and MP2-SAC/6-311G(2d,d,p)[MP2/6-311G(2d,d,p)]///SRP13 for the other low level. However, again we will use simpler notations since there is no possibility of confusion, namely SRP4[MP2]-IC and SRP13[MP2]-IC.

2.3 Kinetic Isotope Effects

The $^{12}\text{C}/^{13}\text{C}$ KIE for the $\text{CH}_4 + \text{Cl}$ reaction is defined in this work as the ratio $^{12}k/^{13}k$ where ^{12}k is the rate constant for the unsubstituted methane, and ^{13}k is that for the substituted isotopomer. In the case of the deuterated reaction, the H/D KIE is the ratio between the rate constants of the unsubstituted and tetradeuterated methane. When the value of the KIE with the rate constant for the lighter isotopomer in the numerator is greater than unity it is called *normal*; otherwise it is called *inverse*.³⁹ Kinetic isotope effects have long been used to infer properties of transition states by assuming that the dynamical bottlenecks of reactions involving different isotopes are the same. In addition tunneling effects are often neglected. However these approximations can lead to significant errors.⁴⁰ In this work neither of these assumptions is made. Instead we use the CVT/G methods discussed in Section 2.2.

3. RESULTS AND DISCUSSION

3.1 Literature Summary

In addition to the work mentioned in the introduction, the reader should note four other recent theoretical studies.

Dobbs and Dixon¹² optimized the saddle point geometry and calculated its frequencies at the MP2/TZ(2d,2d,2p) level, and they calculated a higher-level energy at this geometry by using the QCISD(T)/QZ(3d1f,3d2f,2p1d) level. (TZ and QZ denote triple zeta and quadruple zeta respectively, and QCISD(T) denotes quadratic configuration interaction with perturbation treatment of connected triple substitutions.) They calculated forward reaction rates using conventional TST, including Wigner's lowest-order, unidimensional tunneling correction. With these large basis sets and high levels of theory, they obtained a classical barrier of 8.9 kcal/mol and a zero-point-corrected barrier height of 4.9 kcal/mol. Their final published rate constants, including tunneling corrections as large as 4.4 at 200 K and 1.55 at 300K, are in good agreement with experiment at 500 K but too low by a factor of about 10 at 200 K. In this regard, we note that Wigner's tunneling correction is unjustified when it exceeds \sim 1.5, and it is particularly unreliable for the present heavy-light-heavy mass combination.

Duncan and Truong¹³ calculated the transition state geometry and frequencies by density functional theory (DFT) with a 6-311G(d,p) basis set, and they also used this level to calculate geometries and frequencies along a reaction path. Higher-level energies at the saddle point and along the reaction path were calculated at the PMP4/6-311+G(2df,2pd) level. (PMP4 denotes spin-projected Møller-Plesset fourth-order perturbation theory based on a Hartree-Fock reference wave function.) This yielded a classical barrier height of 7.9 kcal/mol and a zero-point-inclusive barrier height (evaluated at the saddle point) of 3.55 kcal/mol. They calculated the rate constants at a higher level of dynamical theory than previous workers, namely full canonical variational theory with small-curvature tunneling (CVT/SCT), and their final published rate constants are lower than experiment by factors of about 10 and 1.7 at 200 K and at 500 K, respectively.

Espinosa-Garcia and Corchado¹⁴ have carried out rate constant calculations at an even higher dynamical level, namely CVT with canonically optimized multidimensional tunneling (CVT/COMT); in the COMT approach one carries out the thermally averaged

calculations by both SCT and large-curvature-tunneling (LCT) approximations and accepts the larger of the two results. Espinosa-Garcia and Corchado based their calculations on an analytical potential energy surface that they fitted to MP2-SAC calculations reported earlier from our group and to experimental vibrational frequencies. This led to a classical barrier height of 8.1 kcal/mol and a zero-point-corrected barrier height of 4.4 kcal. The resulting calculated rate constants agree with experiment within about 40% over the whole 200–500 K temperature range. One difficulty in comparing the various previous calculations is that apparently only Espinosa-Garcia and Corchado included spin-orbit effects on the reactant partition coefficient correctly. These authors also have reported values of the KIEs for the reaction $\text{CD}_4 + \text{Cl}$; their H/D ratios are too high when compared with the experimental ones.

In a more recent study Jursic¹⁵ reported calculations at different levels of density functional and many-body perturbation theories to obtain the forward and reverse classical barrier and heat of reaction. The best result for the forward and reverse classical barrier heights was achieved at the MP2 level using the 6-311G(2df,p) basis set, which yielded values of 9.0 and 1.9 kcal/mol, respectively. It is difficult to estimate the reliability of these calculations because the geometries were obtained using the 6-31G(d) basis set, which is a small one. In addition the frequencies and zero point vibrational energies (ZPVEs) were not calculated.

3.2 Structural and Energetics Properties

Optimized structures of HCl , CH_3 , and CH_4 were calculated at the highest possible symmetry for each species, i.e., for CH_4 (T_d), CH_3 (D_{3h}), and HCl ($C_{\infty v}$), using the AM1, SRP4, SRP13, and MP2-SAC methods. The resulting bond lengths are compared in Table 1, and the harmonic vibrational frequencies and ZPVEs obtained at the three semiempirical levels and at the two 6-311G(2d,d,p) levels are listed in Table 2. In both tables we also list experimental^{41,42} values for comparison. Although the SRP geometries and vibrational frequencies in these tables are not better than the original AM1 parameter-

ization, when compared to experimental data and ab initio calculations, the SRP surfaces are preferred because of their improved²³ energetics.

Transition state structures and vibrational frequencies are listed in Tables 3 and 4, respectively, together with results obtained by others. The SRP4 and SRP13 surfaces differ significantly as far as the asymmetry of the saddle point geometry. This allows us to test the sensitivity of the results to the geometry of the lower-level surface. The transition state structure as calculated at the MP2-SAC/6-311G(2d,d,p) level is shown in Figure 1. Using the MP2 or MP2-SAC results as a reference, we conclude that the SRP4 and SRP13 calculations yield accurate enough geometries and frequencies to serve as lower levels. We note, however, another significant difference between the SRP4 and SRP13 potential energy surfaces; although the latter is parameterized to give better global properties, the former apparently gives a more accurate imaginary frequency at the saddle point.

It is perhaps of some interest to note the close agreement between the values of the imaginaries frequencies calculated here and the empirical value of $972i\text{ cm}^{-1}$ obtained⁴³ by the BEBO method, although the BEBO method is very sensitive to its parameters, and such agreement cannot be expected in general.

The values for the classical forward barrier (ΔV_f^\ddagger) and reverse barrier (ΔV_r^\ddagger) are listed in Table 5. The unmodified AM1 method gives a negative barrier height, but the AM1-SRP barriers are considerably improved by the adjustment of the NDDO parameters. In Table 6 are the values for the classical forward barrier (ΔV_f^\ddagger), classical endoergicity (ΔE), heat of reaction at 0 K (ΔH_0), and vibrationally adiabatic ground-state barrier height evaluated at the saddle point ($\Delta V_{a,f}^{G\ddagger}$) obtained by the MP2-SAC method. (Note that latter is sometimes called the ZPVE-corrected barrier height.) Equivalent quantities for the reverse reaction are also included along with experimental data⁴⁴⁻⁴⁶ and values inferred^{21a} from experimental data. The theoretical heat of reaction at 298 K was roughly estimated from the calculated values of ΔH_0 by adding 0.6 (the value of RT at 298 K) and we find excellent agreement with the experimental values ($1.89 \pm 0.10\text{ kcal/mol}$).⁴⁴

Transition state vibrational frequencies and the saddle point values of ZPVE for the isotopomers CH_4Cl , $^{13}\text{CH}_4\text{Cl}$, CH_3DCl , CDH_3Cl , and CD_4Cl are listed in Table 7. The saddle point harmonic vibrational frequencies for isotopomers $^{12}\text{CH}_4\text{Cl}$ and $^{13}\text{CH}_4\text{Cl}$ are very similar to each other, showing, for instance, imaginaries frequencies with values of 950i and $940\text{i} \text{ cm}^{-1}$, respectively.

3.3 Chemical Dynamics Results

Figure 2 shows the classical potential energy profile, $V_{MEP}(s)$, and the vibrationally adiabatic ground-state potential curve, $V_a^G(s)$, and Figure 3 illustrates how the geometry varies with s . The present study predicts a variational transition state that is a bit shifted toward the region of the products, for example a value for s_*^{CVT} equal to 0.045 \AA at 300 K in the SRP4-IC calculation and 0.040 \AA at 300 K in the SRP4[MP2]-IC calculation.

In Tables 8 and 9 we compare rate constants calculated by several methods. In the CVT/LCT calculations, the reacting system is allowed to tunnel directly into all energetically accessible vibrationally excited states in the exoergic direction; the transmission coefficient in the endoergic direction is obtained by detailed balance.³⁶ When we use rectilinear coordinates with the SRP4[MP2]-IC implicit potential surface, we find that LCT rate constants are larger than SCT ones. Nevertheless, when the rate constants are calculated at the SRP4-IC or the SRP13[MP2]-IC level, the CVT/SCT rates are larger than at the CVT/LCT ones. These results show that we cannot draw definitive conclusions about the dominant mode of tunneling until we carry out calculations that are converged with respect to the low level for paths that cut across the swath^{28,50,51} region.

In Table 8 we also compare the results of VTST-IC calcualtions using rectilinear and curvilinear coordinates. At the μOMT level, differences are 10–35%. The rate constants obtained using rectilinear coordinates are larger than those calculated with curvilinear coordinates, and they are in better agreement with the experimental results than those calculated using curvilinear coordinates. We assume that such a situation results from a cancellation of errors since curvilinear coordinates are more physical. The rate constants

obtained in the present calculations agree with experiment better than previous calculations,^{12,13,22} but it is not clear to what extent this agreement results from fortuitous cancellation of error. The checks against KIEs (presented below) will provide a more difficult test of theory.

Calculated thermal forward rate constants for the CH₄ + Cl reaction at temperatures from 200 to 1000 K are listed in Table 9 and compared to experimental^{43,45,47,48a} measurements. In Table 9 is also shown how the LCT results change when direct tunneling involving excited vibrational states is or is not included. The experimental results cited as Russell et al.⁴⁵ and DeMore et al.⁴⁷ are fits to various previous experimental studies, which are in excellent agreement. The most recent data are from Pilgrim et al.,^{48a} and their values of the rate constants in the range 400–600 K are in close agreement with the former measurements. The calculations agree with experiment^{43,45,47,48} within a factor of 2.

Various types of tunneling calculations are also possible with an analytic potential energy surface, which, however, is seldom⁴⁹ available for system with many atoms. In the present case, though, an analytic surface was developed by Espinosa-Garcia and Corchado.¹⁴ We can compare our results using rectilinear coordinates to theirs for both SCT and LCT tunneling. Comparing Table 9 of the present paper to Table II of Ref. 14 shows that at the CVT/LCT level, our SRP4[MP2]-IC results and their results agree within a factor decreasing from 2.7 at 200 K to 0.6 at 1000 K. However their data at the LCT level exceed their rates at the SCT level by factors of 14, 7, 4, 3, and 2 at 200, 250, 300, 400, and 500, respectively. As a consequence, their LCT rates exceed ours by factors of 2.7, 1.7, and 1.3 at 200, 250, and 300 K, respectively.

Table 10 shows activation energies computed as local slopes of Arrhenius plots in order to provide the most appropriate comparison to experiment. In the temperature range important for atmospheric chemistry, 200–300 K, the calculated activation energies at the CVT/ μ OMT dynamical level agree with experiment⁴³ within experimental error. Table 10

provides a useful antidote to the still current impression that the experimentally observed activation energy is a good zero-order estimator of the barrier height. Our calculations, with a classical barrier height of 8.0 kcal/mol yield good agreement with experiment for both rate constants and activation energies, even though the experimental activation energy is $4\frac{1}{2}$ - $5\frac{1}{2}$ kcal/mol lower than our classical barrier height.

Calculated rate constants for the reverse reaction, $\text{CH}_3 + \text{HCl}$, are listed in Table 11, where they are compared to the experiments of Russell et al.⁴⁵ Earlier experimental data have been reviewed by Russell et al.⁴⁵ and Pohjonen and Kaskikallio.⁴⁶ Our CVT/ μ OMT values obtained at SRP4[MP2]-IC level are lower than the experimental ones by factors of only 0.9, 1.5, and 1.6 at the temperatures of 300, 400, and 500 K. The theoretical values of the reverse activation energies are shown in Table 12 and are in good agreement with the experimental ones.

Based on either the activation energies or the rate constants, and comparing the present results to those of Refs. 45 and 46, we see that our CVT/ μ OMT systematically underestimate the rate constants and overestimate the activation energy for the forward reaction. Using the results at 400–500 K, where possible errors in the tunneling estimates (due, e.g., to using semiclassical methods or due to intrinsic limitations of the low-level PES calculated at the AM1-SRP level) are less important than at room temperature, one might conclude that the MP2-SAC barrier is high, but only by about 0.2–0.6 kcal/mol. If, however, we accept the results of Ref. 45 for the reverse reaction our barrier height appears to be about 0.5 kcal/mol too low. Since MP2-SAC calculations typically overestimate barrier heights (however, neglect of the spin-orbit effect will partly compensate that systematic error), and since the experimental data is much more consistent for the forward reaction, the former scenario may be more likely. In any event the results agree with experiment with an accuracy that is within or close to the experimental reliability, at least at room temperature and above.

In order to gain a better understanding of the relationship among the various theo-

retical treatments in this and previous studies, we made an attempt to compare them in a consistent fashion, and the results of this analysis are presented in Table 13. First of all, we multiplied the results of Ref. 11 and 12 by the correct multiple-surface bbbbcoefficient to put them on the same basis as the calculations of Ref. 14 and the present paper, which properly include this effect. We do not understand the "spin-orbit correction" of Duncan and Truong,¹³ which is unexpectedly small, in particular equals to 0.03 at 200 K; this appears to be an error. Fortunately those authors published enough information for us to remove the wrong "spin-orbit correction" and include the correct multiple-surface coefficient. We did this for Table 13. Thus all results in Table 13 are based in a correct treatment of the multiple-surface effect. In addition Table 13 compares the various calculations at the level of conventional TST as well as, for each reference, the final (highest) dynamical level of that reference.

First consider the conventional TST results of Table 13. At all the temperatures the conventional TST rate constants are in the order DD < EC < GTT < DT. One might expect that, at the conventional TST level, the rate constants would be ordered in approximately inverse order to the zero-point-corrected barrier height. And in fact, with only one calculation out of order, this is borne out: DD, 4.9 kcal; EC, 4.4 kcal; GTT, 4.8 kcal; DT, 3.55 kcal.

Next consider the effect of higher-level dynamical treatments. Now the calculations divide into two groups. The GTT, DT, and present calculations have $k^{final}/k^{TST} \leq 3$ at 200 K and have $0.7 \leq k^{final}/k^{TST} \leq 1.6$ at 300 - 1000 K. The other two calculations show much larger dynamical effects. This is perhaps not surprising for the DD calculation since the one-dimensional tunneling calculation they used is known to be unreliable. The results of Espinosa-Garcia and Corchado are more surprising because they found that the LCT tunnneling result is a factor of 75 at 200 K, whereas our results for that radio (see table 13) range from 2.9 to 7.3, depending on which low-level surface and which high-level frequencies are used. Resolution of this discrepancy would be an interesting subject for

further work.

3.4 Kinetic Isotope Effects

Values of the theoretical $^{12}\text{C}/^{13}\text{C}$ KIEs for the forward reaction are listed in Table 14. There is limited experimental data with which to compare our calculations, but nevertheless these data provide a critical test of the correctness of our model. In particular we see that the present calculations are in reasonably good agreement with the available experimental results, especially as compared to conventional TST or TST with the Wigner correction. The calculations using MP2 frequencies agree with experiment better than those with MP2-SAC frequencies. It is therefore an open question whether the SAC approach, which is very successful for improving energy predictions along a reaction path, should also be used for frequencies.

The conventional TST results for the $^{12}\text{C}/^{13}\text{C}$ KIEs in the present study are reasonably similar to the conventional TST results calculated by Tanaka et al.^{9a} at the MP2/6-311G(3d,2p) level. In particular, at the conventional TST level, our calculated KIE decreases from 1.028 to 1.021 over the 200 to 300 K range, whereas their value is about 0.006 smaller over the whole temperatures interval. They neglected variational effects and made a one-dimensional tunneling correction that increases their calculated KIE by about 0.006, as a consequence of which it agrees very well with our uncorrected TST value. But since variational effects and multidimensional tunneling effects are significant, our conventional TST results and their results both underestimate the KIEs by about 4%.

In the case of AM1-IC, exploratory calculations (not tabulated here) show that the original NDDO parameterization predicts an inverse kinetic isotope effect for the $^{12}\text{C}/^{13}\text{C}$ KIE process at the CVT level, and from these results we can conclude that AM1 method without reparameterization is not accurate and reliable enough to study this present reaction. This provides a dramatic example of the power of the SRP approach.

The kinetics of the reaction $\text{CH}_3\text{D} + \text{Cl}$ are controlled by the contributions of two partial reactions. One reaction is $\text{CH}_3\text{D} + \text{Cl} \rightleftharpoons \text{DCl} + \text{CH}_3$ with symmetry numbers³¹

3 and 2 for the forward and reverse directions, respectively, and with a transition state ClDCH_3 (See Table 7) which belongs to the point group C_{3v} . The second partial reaction is $\text{CH}_3\text{D} + \text{Cl} \rightleftharpoons \text{CH}_2\text{D} + \text{HCl}$ with symmetry numbers 1 and 2, and with the transition structure ClHCDH_2 with vibrational symmetry C_s . The total rate constant corresponds to the sum of these two partial reactions. The values of the deuterium kinetic isotopic effects are shown in Table 14. It is encouraging to see the agreement between our theoretical results and the experimental results⁵ because the measurements were performed using tunable laser infrared spectroscopy, which is a very accurate experimental technique. Table 14 also gives the result of another experiment⁴ at 295 K, and it is also encouraging that our results fall between the two experimental results.

Calculations for the reaction $\text{CD}_4 + \text{Cl}$ are also reported in the Table 14. This reaction show a high kinetic isotope effect, and our results are in reasonably good agreement with the available experiments data. In footnote *d* of Table 14 are given the corresponding results obtained by Espinosa-Garcia and Corchado¹⁴ using their analytical potential energy surface, and the agreement with experiment is significantly poorer.

Table 15 summarizes the mean unsigned errors in comparison to experiment at the four temperatures. Clearly the major improvement in the predicted KIEs occurs at the CVT level where variational optimization of the location of the dynamical bottleneck is included. Inclusion of tunneling effects provides no consistent improvement in the KIEs.

4. CONCLUSIONS

We can explain the $^{12}\text{C}/^{13}\text{C}$ KIEs in the heavy-light-heavy $\text{CH}_4 + \text{Cl}$ reaction by dual-level variational transition state theory with optimized multidimensional tunneling contributions. The higher level is an MP2-SAC calculation with a well balanced basis set. The results also show the power of adjusting the NDDO parameters of a low-level calculation to calculate energetic and structural properties accurately, and they demonstrate the usefulness of the evolutionary algorithm approach for simultaneous optimization of a large set of variables. Conventional TST gives larger errors not only for $^{12}\text{C}/^{13}\text{C}$ kinetic isotope

effects, but also for CH₄/CD₄ kinetic isotope effects. We hope these calculations will be useful in modeling the chemistry of methane gas in the atmosphere and also for advancing the methodology of *ab initio* chemical kinetics for atmospheric and combustion reactions in general.

ACKNOWLEDGMENTS

The authors are grateful to Xavier Assfeld for modifying GAUSSIAN 94 to allow the calculation of SAC gradients. One of us (O.R.N.) thanks the members of the Truhlar group for their hospitality during his postdoctoral stage and the Fundação de Amparo a Pesquisa do Estado de São Paulo (FAPESP) for a fellowship. This research was supported in part by the U.S. Department of Energy, office of Basic Sciences under grant 86ER-13579.

REFERENCES

- (1) Brenninkmeijer, C. A. M.; Lowe, D. C.; Manning, M. R.; Sparks R. J.; van Velthoven, P. F. J. *J. Geophys. Res.* **1995**, 100 D, 26163.
- (2) Crutzen, P. J. *Ambio* **1995**, 24, 52.
- (3) (a) Cantrell C. A., Shetter R. E., Mc Daniel A. H., Calvert J. G., Davidson J. A., Lowe D. C., Tyler S. C., Cicerone R. J.; Greenberg J. P., *J. Geophys. Res.* **1990**, 95, 22455. (b) Saueressig, G; Bergamaschi, P.; Crowley, J. N.; Fisher H.; Harris, G. W. *Geophys. Res. Lett.* **1995**, 22, 1225. (c) Bergamaschi, P.; Brühl, C.; Brenninkmeijer, C. A. M.; Saueressig, G.; Crowley, G. N.; Groß, J. U.; Fisher, H.; Crutzen, P. J. *Geophys. Res. Lett.*, **1996**, 23, 2227.
- (4) Wallington, T. J.; Hurley, M. D. *Chem. Phys. Lett.* **1992**, 189, 437.
- (5) Saueressig, G.; Bergamaschi, P.; Crowley, J. N.; Fisher, H.; Harris, G. W. *Geophys. Res. Lett.* **1996**, 23, 3619.
- (6) Matsumi, Y; Izumi, K.; Skorokdov, V; Kawasaki, M.; Tanaka, N. *J. Phys. Chem. A*, **1997**, 101, 1216.
- (7) Chiltz, G.; Eckling, R.; Goldfinger, P.; Huybrechts, G.; Johnston, H. S.; Meyers, L.; Verbeke, G. *J. Chem. Phys.* **1963**, 5, 1053.
- (8) See, for instance: (a) Lu, D.-h; Maurice, D.; Truhlar, D. G. *J. Am. Chem. Soc.* **1990**, 112, 6206; (b) Liu, Y.-P.; Lynch, G. C.; Truong, T. N.; Lu, D.-h.; Truhlar, D. G.; Garrett, B. C. *J. Am. Chem. Soc.* **1993**, 115, 2408; (c) Melissas, V. S.; Truhlar, D. G. *J. Chem. Phys.* **1993**, 99, 3542.
- (9) (a) Tanaka, N; Xiao, Y.; Lasaga, A. C. *J. Atmos. Chem.* **1996**, 23, 37; (b) Chen, Y.; Rauk, A.; Tschaikow-Roux, E. *J. Phys. Chem.* **1991**, 95, 9900.
- (10) Truong, T. N.; Baldridge, K. K.; Gordon, M. S.; Steckler, R.; Truhlar, D. G. *J. Chem. Phys.* **1989**, 90, 7137.
- (11) Gonzalez-Lafont, A.; Truong, T. N.; Truhlar, D. G. *J. Chem. Phys.* **1991**, 95, 8875.

- (12) Dobbs, K. D.; Dixon, D. A. *J. Phys. Chem.* **1994**, *98*, 12584.
- (13) Duncan, W. T.; Truong, T. N. *J. Chem. Phys.* **1995**, *103*, 9642 .
- (14) Espinosa-Garcia, J.; Corchado, J. C. *J. Chem. Phys.* **1996**, *105*, 3517.
- (15) Jursic, B. S., *Chem. Phys. Lett.*, **1997**, *264*, 113.
- (16) Chuang, Y. -Y.; Truhlar, D. G. *J. Phys. Chem. A* **1997**, *101*, 3808.
- (17) Hu, W.-P.; Liu, Y.-P.; Truhlar, D. G. *J. Chem. Faraday Trans.* **1994**, *90*, 1715.
- (18) Truhlar, D. G. in *The Reaction Path in Chemistry: Current Approaches and Perspectives*, edited by D. Heidrich (Kluwer, Dordrecht, 1995), pp. 229-255.
- (19) Corchado, J. C.; Espinosa-Garcia, J.; Hu, W.-P.; Rossi, I; Truhlar, D. G. *J. Phys. Chem.* **1995**, *99*, 687.
- (20) (a) Krishnan, R.; Binkley, J. S.; Seeger, R.; Pople, J. A. *J. Chem. Phys.* **1980**, *72*, 650; (b) McLean, A. D.; Chandler, G. S. *J. Chem. Phys.* **1980**, *72*, 5639.
- (21) (a) Gordon, M. S.; Truhlar, D. G. *J. Am Chem. Soc.* **1986**, *108*, 542; (b) Gordon, M. S.; Truhlar, D. G. *Int. J. Quant. Chem.* **1987**, *31*, 81; (c) Gordon, M. S.; Nguyen, K. A.; Truhlar, D. G.; *J. Phys. Chem.* **1989**, *93*, 7356. (d) Rossi, I.; Truhlar, D. G. *Chem. Phys. Lett.* **1995**, *234*, 64.
- (22) Gonzalez-Lafont, A.; Truong, T. N.; Truhlar, D. G. *J. Phys. Chem.* **1991**, *95*, 4618.
- (23) Rossi, I.; Truhlar, D. G. *Chem. Phys. Lett.* **1995**, *233*, 231.
- (24) Chuang, Y.-P.; Hu, W.-P.; Lynch, G. C.; Liu, Y.-P.; Truhlar, D. G. MORATE–version 7.4YC, University of Minnesota, Minneapolis, 1997.
- (25) Stewart, J. J. P.; Rossi, I.; Hu, W.-P.; Lynch, G. C.; Liu, Y.-P.; Truhlar, D. G. MOPAC–version 5.05mn, University of Minnesota, 1995.
- (26) Steckler, R.; Chuang, Y. -Y.; Fast, P. L.; Coitiño, E. L.; Corchado, J. C.; Hu, W.-P.; Lu, Y.-P.; Liu, Y.-P.; Lynch, G. C.; Nguyen, K. A.; Jackels, C. F.; Gu, Z. M.; Rossi, I; Clayton, S.; Melissas, V. S.; Garrett, B. C.; Isaacson, A. D.; Truhlar, D. G. POLYRATE–version 7.4, University of Minnesota, Minneapolis, 1997.

- (27) (a) Frisch, M. J.; Trucks, G. W.; Schlegel, H. B.; Gill, P. M. W.; Johnson, B. G.; Robb, M. A.; Cheeseman, J. R.; Keith, T.; Peterson, G. A.; Montgomery, J. A.; Raghavachari, K.; Al-Laham, M. A.; Zakrzewski, V. G.; Ortiz, J. V.; Foresman, J. B.; Cioslowski, J.; Stefanov, B. B.; Nanayakkara, A.; Challacombe, M.; Peng, C. Y.; Ayala, P.Y.; Chen, W.; Wong, M. W.; Andres, J. L.; Replogle, E. S.; Gomperts, R.; Martin, R. L.; Fox, D. J.; Binkley, J. S.; Defrees, D. J.; Baker, J.; Stewart, J. P.; Head-Gordon, M.; Gonzalez, C.; Pople, J. A. GAUSSIAN 94-Revision B.1, Gaussian, Inc, Pittsburgh, 1995. (b) Assfeld, X.; Truhlar, D. G. unpublished.
- (28) Truhlar, D. G.; Isaacson, A. D.; Garrett, B. C. in *The Theory of Chemical Reaction Dynamics*, edited by Baer, M. (CRC Press, Boca Raton, Florida, 1985), Vol. 4, pp. 65-137.
- (29) Garrett, B. C.; Redmon, M. J.; Steckler, R.; Truhlar, D. G.; Gordon, M. S.; Baldridge, K. K.; Bartol, D. *J. Phys. Chem.* **1988**, 88, 1476.
- (30) See for instance: Steinfeld, J. I.; Francisco, J. S.; Hase, W. L. *Chemical Kinetics and Dynamics*, Prentice Hall, Englewood Cliffs: New Jersey; 1989, pp. 326.
- (31) Moore, C. E. *Atomic Energy Levels*, Nat. Stand. Ref. Data Ser., Nat. Bur. Stand (US), Vol. II, 1971.
- (32) Truhlar, D. G. *J. Chem. Phys.* **1972**, 56, 3189; **1972**, 61, 440 (E).
- (33) Stark, K.; Werner, H.-J. *J. Chem. Phys.* **1996**, 104, 6515.
- (34) Garrett, B. C.; Truhlar, D. G.; Grev, R. S.; Magnuson, A. W. *J. Phys. Chem.* **1980**, 84, 1730.
- (35) Truhlar, D. G.; Kuppermann, A. *J. Am. Chem. Soc.* **1971**, 93, 1840.
- (36) (a) Liu, D.-h.; Truong, T. N.; Melissas, V. S.; Lynch, G. C.; Liu, Y.-P.; Garrett, B. C.; Steckler, R.; Isaacson, A. D.; Rai, S. N.; Hancock, G. C.; Lauderdale, J. C.; Joseph, T.; Truhlar, D. G. *Computer Phys. Commun.* **1992**, 71, 235. (b) Truong, T. N.; Lu, D.-h.; Lynch, G. C.; Liu, Y.-P.; Melissas, V. S.; Stewart, J. J. P.; Steckler, R.; Garrett, B. C.; Isaacson, A. D.; Gonzalez-Lafont, A.; Rai, S. N.; Hancock, G. C.;

- Joseph, T.; Truhlar, D. G. *Computer Phys. Commun.* **1993**, *75*, 143.
- (37) Liu, Y.-P.; Lu, D.-h.; Gonzalez-Lafont, A.; Truhlar, D. G.; Garrett, B. C. *J. Am. Chem. Soc.* **1993**, *115*, 7806.
- (38) (a) Jackels, C. F.; Gu, Z.; Truhlar, D. G. *J. Chem. Phys.* **1995**, *102*, 3188. (b) Nguyen, K. A.; Jackels, C. F.; Truhlar, D. G. *J. Chem. Phys.* **1996**, *104*, 6491. (c) Chuang, Y.-Y., Truhlar, D. G. *J. Phys. Chem.* **1997**, *107*, 83. (d) Chuang, Y. -Y.; Truhlar, D. G. *J. Phys. Chem.*, in press.
- (39) Melander, L.; Saunders W. H. Jr. *Reaction Rates of Isotopic Molecules*, 2nd ed., Wiley-Interscience Publication, New York, 1980.
- (40) (a) Truhlar, D. G.; Lu, D.-h.; Tucker, S. C.; Zhao, X. G.; Gonzalez-Lafont, A.; Truong, T. N.; Maurice, D.; Liu, Y.-P.; Lynch, G. C. *ACS Symp. Ser.* **1992**, *502*, 16. (b) Truhlar, D. G., Garrett, B. C.; Klippenstein, S. J. *J. Phys. Chem.* **1996**, *100*, 12771. (c) Allison, T. C; Truhlar, D. G. in *Modern Methods for Multidimensional Dynamics Computational in Chemistry*; Thompson, D. L., Ed.; World Scientific: Singapore; in press.
- (41) Herzberg, G.; Huber, K. B. *Molecular Spectra and Molecular Structure. IV. Constants of Diatomic Molecules*, Vol. 4 (van Nostrand, Princeton, New Jersey, 1979).
- (42) *JANAF Thermochemical Tables*, edited by Chase, M. W. Jr.; Davies, C. A.; Dowley. J. R. Jr.; Frurip, D. J.; McDonald, R. A. (Natl. Standar Ref. Data Ser. Natl. Bur. Stand., 1985), Vol. 14.
- (43) Zahniser, M. S.; Berquist, B. M.; Kaufman, F. *Int. J. Chem. Kinet.* **1978**, *10*, 15.
- (44) Dobbis, O; Benson, S. W. *Int. J. Chem. Kinet.* **1987**, *19*, 691.
- (45) Russell, J. J.; Seetula, J. A.; Senkan, S. M.; Gutman, D. *Int. J. Chem. Kinet.* **1988**, *20*, 759.
- (46) Pohjonen, P. -L.; Koskikallio, J. *Acta Chem. Scand. A* **1979**, *33*, 449.
- (47) DeMore, W. B.; Sander, S. P.; Golden, D. M.; Hampson, R. F.; Kurylo, M. J.;

- Howard, C. J.; Ravishankara, A. R.; Kob, C. E.; Molina, M. J. in *JPL Publication 92-20*, Jet Propulsion Laboratory, Pasadena, CA, 1992.
- (48) (a) Pilgrim, J. S.; McIlroy, A.; Taatjes, C. A. *J. Phys. A*, **1997**, 33, 1873. (b) Seeley, J. V., Jayme, J. T.; Molina, M. J. *J. Phys. Chem.* **1996**, 100, 4019.
- (49) Truhlar, D. G.; Steckler, R.; Gordon, M. S. *Chem. Rev.* **1987**, 87, 217.
- (50) Kreevoy, M. M.; Ostović, D.; Truhlar, D. G.; Garrett, B. C. *J. Phys. Chem.* **1986**, 90, 3766.
- (51) Truhlar, D. G.; Gordon, M. S. *Science* **1990**, 249, 491.

Table 1. Optimized bond lengths in Å.

Species	Bond	AM1	SRP4	SRP13	MP2 ^a	MP2-SAC ^a	Exp.
HCl(C _{∞v})	H-Cl	1.284	1.296	1.289	1.275	1.276	1.274 ^b
CH ₃ (D _{3h})	C-H	1.080	1.087	1.087	1.079	1.080	1.079 ^c
CH ₄ (T _d)	C-H	1.112	1.106	1.105	1.089	1.091	1.091

^aValues already reported in Ref. 10 ^bRef. 41 ^cRef. 42Table 2. Harmonic normal-mode vibrational frequencies (in cm⁻¹) and ZPVE energies (kcal/mol) for the species CH₄, CH₃, and HCl.

Species	Mode	Exp.	AM1	SRP4	SRP13	MP2 ^a	MP2-SAC
HCl	σ	2991 ^b	2658	2641	2589	3048	3030
	ZPVE	4.3	3.8	3.8	3.8	4.4	4.3
CH ₃	a' ₁	3002 ^b	3252	3291	3285	3176	3165
	a' ₂	580	780	961	1043	426	436
	e'	3184	3249	3293	3260	3369	3361
	e'	1383	1348	1306	1268	1452	1441
	ZPVE	18.2	18.9	19.2	19.1	18.9	16.9
CH ₄	a ₁	2917 ^c	3216	3297	3303	3080	3065
	e	1534	1412	1324	1236	1582	1565
	t ₁	3019	3189	3162	3162	3218	3210
	t ₂	1306	1380	1372	1367	1364	1346
	ZPVE	27.1	27.9	28.1	27.7	28.6	25.4

^aValues already reported in Ref. 10 ^bRef. 41 ^cRef. 42

Table 3. Transition state structures^a.

Methods	R ₁	R ₂	R ₃	α
AM1	1.540	1.264	1.104	104.4
SRP4	1.500	1.398	1.096	99.4
SRP13	1.410	1.411	1.098	100.4
MP2/TZ+2P ^b	1.375	1.452	1.078	101.2
DFT/6-311G(d,p) ^c	1.431	1.443	1.077	100.6
MP2 ^d	1.447	1.370	1.085	101.6
MP2-SAC ^d	1.431	1.388	1.086	101.2

^aR1, R2, and R3 are respectively the Cl-H(4) and, H(4)-C(1), and C-H(2) distances in Å, and α is the H(4)-C-H(2) bond angle in degrees; see Figure 1 for a precise specification. The transition state has C_{3v} symmetry ^bRef. 12 ^cRef. 13 ^dCalculations with the 6-311G(2d,d,p) basis set; these were first reported in Ref. 10.

Table 4. Comparison of the values for the transition state vibrational frequencies (cm^{-1}) and ZPVE (kcal/mol) obtained here and by Espinosa-Garcia and Corchado,¹⁴ Dobbs and Dixon,¹² and Duncan and Truong.¹³

Mode	MP2-SAC ^a	MP2 ^a	AM1	SRP4	SRP13	APES ^b	MP2 ^c	BH&HLYP ^d
$\nu_1(\text{a}')$	3118	3131	3189	3258	3238	2960	3132	3162
$\nu_2(\text{a}')$	1227	1223	1441	1452	1446	1190	1213	1211
$\nu_3(\text{a}')$	572	519	496	604	536	543	511	541
$\nu_4(\text{e})$	3295	3303	3144	3238	3191	3022	3305	3328
$\nu_5(\text{e})$	1441	1457	1360	1311	1274	1419	1448	1468
$\nu_6(\text{e})$	874	923	1094	794	805	1102	958	920
$\nu_7(\text{e})$	324	337	190	174	140	344	378	385
$\nu_8(\text{a}')$	950i	1163i	922i	943i	1163i	1196i	1262i	996i
ZPVE	24.0	24.2	23.9	23.4	22.9	—	—	—

^aCalculations with the 6-311G(2d,d,p) basis set as already reported in Ref. 10.

^bAnalytical Potential Energy Surface; Ref. 14.

^cCalculated using a (TZ + P) basis set; Ref. 12.

^dDensity functional theory with Becke's half-and-half exchange and Lee-Yang-Parr non-local correlation functional using the 6-311(d,p) basis set; Ref. 13.

Table 5. Values of the forward (ΔV_f^\ddagger) and reverse (ΔV_r^\ddagger) classical barriers (in kcal/mol) using the AM1, AM1-SRP, and MP2-SAC methods.

Barriers	AM1	SRP4	SRP13	MP2-SAC
ΔV_f^\ddagger	-6.30	10.86	10.10	7.96
ΔV_r^\ddagger	-8.56	1.08	1.02	1.20

Table 6. Energetic properties (in kcal/mol) of the reaction.

	MP2-SAC ^a	Exp.:
ΔE	6.79	6.40 ^b
ΔH_0	1.20	—
ΔH_{298}	1.80	1.89 ^c
ΔV_f^\ddagger	7.96	—
$\Delta V_{a,f}^{G\ddagger}$	3.56	3.5 ^d
ΔV_r^\ddagger	1.17	—
$\Delta V_{a,r}^{G\ddagger}$	1.96	1.5 ^e

^aSince the results in this table involve only stationary points, the AM1-IC, SRP4-IC, and SRP13-IC results are all identical to the MP2-SAC ones.

^bRef. 21a ^cRef. 44 ^dRef. 43 ^eRef. 45

Table 7. Transition state vibrational frequencies (cm^{-1}) and ZPVE (in kcal/mol) for the isotopomers CH_4Cl , $^{13}\text{CH}_4\text{Cl}$, CH_3DCl , CDH_3Cl and CD_4Cl .

Mode	MP2-SAC				MP2			
	ClHCH_3	$\text{ClH}^{13}\text{CH}_3$	ClDCH_3	ClDCD_3	ClHCH_3	$\text{ClH}^{13}\text{CH}_3$	ClDCH_3	ClDCD_3
$\nu_1(\text{a}')$	3118	3117	3115	2214	3131	3130	3131	2224
$\nu_2(\text{a}')$	1227	1218	1147	1056	1224	1215	1166	949
$\nu_3(\text{a}')$	572	565	553	484	519	511	510	458
$\nu_4(\text{e})$	3295	3282	3293	2451	3303	3290	3303	2457
$\nu_5(\text{e})$	1441	1436	1440	956	1457	1452	1457	1067
$\nu_6(\text{e})$	874	872	738	631	923	921	781	667
$\nu_7(\text{e})$	324	266	324	232	336	336	284	240
$\nu_{\ddagger}(\text{a}')$	950i	940i	748i	746i	1162i	1155i	888i	881i
ZPVE	24.0	21.4	20.8	15.8	24.2	21.4	21.0	16.0

	MP2-SAC		MP2
	ClHCDH_2	ClHCDH_2	ClHCDH_2
ν_1	3295		3303
ν_2	3188		3199
ν_3	2362		2370
ν_4	1429		1445
ν_5	1214		1229
ν_6	1174		1165
ν_7	873		921
ν_8	815		855
ν_9	550		506
ν_{10}	323		334
ν_{11}	274		284
ν_{\ddagger}	946i		1158i
ZPVE	19.8		19.9

Table 8. Forward rate constants for the $\text{CH}_4 + \text{Cl}$ reaction using the AM1-SRP4 and AM1-SRP13 sets of parameters, rectilinear and curvilinear coordinates.^a

	TST	CVT	ZCT	T ^b	μOMT^c	CVT	ZCT	T ^b	μOMT^c	
	Rectilinear					Curvilinear				
SRP4-IC										
200	2.0(-15)	1.2(-15)	3.0(-15)	3.7(-15)	5.4(-15)	9.4(-16)	2.5(-15)	2.9(-15)	4.0(-15)	
300	4.5(-14)	3.1(-14)	4.8(-14)	5.3(-14)	6.7(-14)	2.7(-14)	4.2(-14)	4.6(-14)	5.5(-14)	
500	8.1(-13)	6.4(-13)	7.5(-13)	7.7(-13)	8.5(-13)	5.8(-13)	6.8(-13)	7.0(-13)	7.6(-13)	
SRP4[MP2]-IC										
200	1.9(-15)	1.3(-15)	3.3(-15)	5.4(-15)	5.6(-15)	1.1(-15)	2.7(-15)	4.3(-15)	4.4(-15)	
300	4.4(-14)	3.4(-14)	5.1(-14)	6.7(-14)	6.9(-14)	3.0(-14)	4.5(-14)	5.8(-14)	5.9(-14)	
500	7.9(-13)	6.5(-13)	7.6(-13)	8.5(-13)	8.6(-13)	5.9(-13)	6.9(-13)	7.7(-13)	7.8(-13)	
SRP13[MP2]-IC										
200	1.9(-15)	1.9(-15)	5.8(-15)	1.2(-14)	1.4(-14)	1.8(-15)	4.7(-15)	9.7(-15)	1.1(-14)	
300	4.4(-14)	4.4(-14)	7.1(-14)	1.1(-13)	1.2(-13)	4.1(-14)	6.2(-14)	9.1(-14)	9.7(-14)	
500	7.9(-13)	7.9(-13)	9.3(-13)	1.1(-12)	1.1(-12)	7.1(-13)	8.3(-13)	9.6(-13)	9.9(-13)	

^aIn tables, to save space, ZCT denotes CVT/ZCT, SCT denotes CVT/SCT, LCT denotes CVT/LCT, and μOMT denotes CVT/ μOMT ^bThe T column gives LCT results for SRP4-IC and SRP13[MP2]-IC, and it gives SCT results for SRP4[MP2]-IC ^c μOMT is identical (to 3 significant figures) to SCT for SRP4-IC and SRP13[MP2]-IC and to LCT for SRP4[MP2]-IC.

Table 9. Forward rate constants for the $\text{CH}_4 + \text{Cl}$ reaction from calculations and from experiment.

T (K)	TST	CVT	ZCT	SCT	μOMT^a	Ref. 43	Ref. 45	Ref. 47	Ref. 48a
	Rectilinear, SRP4[MP2]-IC					Experiment			
200	1.9(-15)	1.3(-15)	3.3(-15)	5.4(-15)	5.6(-15)	1.1(-14)	—	1.1(-14)	—
						3.9(-15) ^b			
250	1.2(-14)	9.0(-15)	1.6(-14)	2.3(-14)	2.4(-14)	4.1(-14)	—	4.3(-14)	—
						1.8(-14) ^b			
300	4.4(-14)	3.4(-14)	5.1(-14)	6.7(-14)	6.9(-14)	1.0(-13)	9.4(-14)	1.0(-13)	9.3(-14)
						5.5(-14) ^b			
400	2.5(-13)	2.0(-13)	2.5(-13)	3.0(-13)	3.1(-13)	3.5(-13)	3.4(-13)	3.1(-13)	3.0(-13)
						2.6(-13) ^b			
500	7.9(-13)	6.5(-13)	7.6(-13)	8.5(-13)	8.6(-13)	8.8(-13)	7.5(-13)	8.2(-13)	6.5(-13)
						7.8(-13) ^b			
600	1.9(-12)	1.6(-12)	1.7(-12)	1.9(-12)	1.9(-12)	—	—	—	1.7(-12)
						1.8(-12) ^b			
1000	1.5(-11)	1.3(-11)	1.4(-11)	1.4(-11)	1.4(-11) ^b	—	—	—	—
						1.4(-11)			

^a For all cases in this table, CVT/LCT and CVT/ μOMT are identical to three significant figures.

^b The lower entry is the result obtained by CVT/LCT or CVT/ μOMT if tunneling is allowed only into the vibrational ground state in the exoergic direction of reaction.

Table 10. Forward activation energies (kcal/mol).

	T (K)			
	200 - 300	300 - 500	500 - 600	1000 - 1500
SRP4[MP2]-IC				
CVT	3.86	4.41	5.21	8.33
CVT/ZCT	3.28	4.02	4.94	8.20
CVT/SCT	3.01	3.78	4.74	8.10
CVT/LCT	2.99	3.76	4.72	8.09
CVT/ μ OMT	2.99	3.76	4.72	8.09
SRP13[MP2]-IC				
CVT	3.72	4.30	5.12	8.08
CVT/ZCT	3.00	3.84	4.78	7.99
CVT/SCT	2.55	3.42	4.44	7.81
CVT/LCT	2.59	3.48	4.50	7.85
CVT/ μ OMT	2.55	3.42	4.44	7.81
IVTST ^a				
TST	3.70	4.35	5.20	8.90
CVT/2GP	3.90	4.50	5.25	8.25
CVT/ZCT-2GP	3.50	4.10	5.20	8.10
CVT/SCT-2GP	3.30	4.00	4.70	7.90
Experimental				
Ref. 43	2.6±0.4	3.5±0.5	—	—
Ref. 45	—	3.1±0.3	—	—

^aRef. 11

Table 11. Reverse rate constants (in rectilinear coordinates) for the HCl + CH₃ reaction at two levels of calculations and experimental values.

T(K)	TST	CVT	Theory				Experiment	
			ZCT	SCT	LCT	μ OMT	Ref. 45	Ref. 46
SRP4[MP2]-IC								
200	1.1(-14)	7.8(-15)	1.9(-14)	3.2(-14)	3.3(-14)	3.3(-14)	—	—
250	2.6(-14)	1.9(-14)	3.4(-14)	4.9(-14)	5.1(-14)	5.1(-14)	—	—
300	4.5(-14)	3.4(-14)	5.2(-14)	6.9(-14)	7.0(-14)	7.0(-14)	4.8(-14)	6.6(-14)
400	9.3(-13)	7.5(-14)	9.5(-14)	1.1(-13)	1.1(-13)	1.1(-13)	8.6(-14)	1.6(-13)
500	1.5(-13)	1.3(-13)	1.5(-13)	1.7(-13)	1.7(-13)	1.7(-13)	1.2(-13)	2.8(-13)
600	2.3(-13)	1.9(-13)	2.1(-13)	2.3(-13)	2.3(-13)	2.3(-13)	—	—
1000	7.1(-13)	6.0(-13)	6.3(-13)	6.5(-13)	6.5(-13)	6.5(-13)	—	—
SRP13[MP2]-IC								
200	1.1(-14)	1.1(-14)	3.4(-14)	7.9(-14)	7.1(-14)	7.9(-14)	—	—
250	2.6(-14)	2.6(-14)	5.2(-14)	9.8(-14)	8.9(-14)	9.8(-14)	—	—
300	4.5(-14)	4.5(-14)	7.3(-14)	1.2(-13)	1.1(-13)	1.2(-13)	4.8(-14)	6.6(-14)
400	9.3(-13)	9.3(-14)	1.2(-13)	1.6(-13)	1.6(-13)	1.6(-13)	8.6(-14)	1.6(-13)
500	1.5(-13)	1.5(-13)	1.8(-13)	2.2(-13)	2.1(-13)	2.2(-13)	1.2(-13)	2.8(-13)
1000	7.1(-13)	6.6(-13)	6.7(-13)	7.1(-13)	7.0(-13)	7.1(-13)	—	—

Table 12. Reverse activation energies (kcal/mol).

	T(K)		
	250 - 350	500 - 600	1000 - 1500
SRP4[MP2]-IC			
CVT	1.77	2.44	5.72
CVT/ZCT	1.31	2.16	5.59
CVT/SCT	1.04	1.97	5.48
CVT/LCT	1.02	1.95	5.48
CVT/ μ OMT	1.02	1.95	5.48
SRP13[MP2]-IC			
CVT	1.67	2.35	5.47
CVT/ZCT	1.07	2.01	5.38
CVT/SCT	0.63	1.67	5.20
CVT/LCT	0.68	1.76	5.24
CVT/ μ OMT	0.63	1.67	5.20
Experimental			
Ref. 45	1.4 ^a		

^a296–495 K

Table 13. Theoretical forward rate constants ($\text{cm}^3 \text{ molecule}^{-1} \text{s}^{-1}$).

T(K)	k^{TST}				k^{final}				k^{final}/k^{TST}							
	GTT	This ^{a,b}	DD ^c	DT ^d	EC ^e	GTT ^a	DD ^c	DT ^d	EC ^c	This	GTT	DD	DT	EC	This	
200	1.9(-15)	2.8(-17)	5.9(-15)	2.0(-16)	3.1(-15)	5.0(-16)	1.8(-14)	1.5(-14)	5.6(-15)	1.6	18	3.0	75	2.9		
300	4.4(-14)	1.6(-15)	7.7(-14)	9.4(-15)	4.9(-14)	1.7(-14)	1.2(-13)	8.8(-14)	6.9(-14)	1.1	10.1	1.6	9.4	1.6		
500	7.9(-13)	6.3(-14)	8.1(-13)	2.8(-13)	7.1(-13)	3.9(-13)	9.3(-13)	6.4(-13)	8.8(-13)	0.9	6.2	1.2	2.3	1.1		
1000	1.5(-11)	n.r. ^f	1.0(-11)	7.4(-12)	1.1(-11)	n.r.	1.0(-11)	8.2(-12)	1.4(-11)	0.7	n.r.	1.1	1.1	0.9		

^aRef. 11 with rate constants multiplied by eq.(3).^bAt the level of conventional TST the present results (which are labeled "This") are identical to those of Ref. 11 when the multiple-surface coefficient is included in both calculations.^cRef. 12 with rate constants multiplicatied by eq. (3).^dRef. 13 with "no S.O. coupling" results multiplicatied by eq.(3).^eRef. 14.^fn.r. = not reported.

Table 14. Values of the kinetic isotope effects for hydrogen abstraction from the $^{13}\text{CH}_4$, CH_3D , and CD_4 by chlorine atoms at the AM1-SRP4[MP2]-IC level of calculation.

T (K)	TST	TST/W	CVT	ZCT	SCT	LCT	μOMT	Exp.
$(^{12}\text{CH}_4 + \text{Cl})/(^{13}\text{CH}_4 + \text{Cl})$								
200	1.028	1.037	1.067	1.085	1.114	1.091	1.091	—
223	1.026	1.034	1.061	1.075	1.099	1.080	1.080	1.075 ± 0.005^a
243	1.024	1.032	1.057	1.068	1.090	1.072	1.072	1.069 ± 0.004^a
263	1.023	1.031	1.054	1.063	1.082	1.066	1.066	1.070 ± 0.004^a
297	1.021	1.028	1.049	1.056	1.072	1.057	1.057	1.066 ± 0.002^a
500	1.013	1.017	1.033	1.035	1.041	1.035	1.035	—
1000	1.006	1.007	1.023	1.023	1.025	1.023	1.023	—
$(\text{CH}_4 + \text{Cl})/(\text{CH}_3\text{D} + \text{Cl})$								
200	1.51	1.52	1.60	1.64	1.66	1.51	1.51	—
223	1.48	1.50	1.55	1.64	1.60	1.47	1.47	1.59 ± 0.06^b
243	1.46	1.48	1.52	1.54	1.55	1.44	1.44	1.59 ± 0.05^b
263	1.45	1.46	1.49	1.50	1.51	1.42	1.42	1.57 ± 0.05^b
296	1.42	1.43	1.44	1.45	1.45	1.38	1.38	1.51 ± 0.04^c
300	1.41	1.43	1.44	1.45	1.45	1.38	1.38	—
500	1.28	1.30	1.25	1.26	1.25	1.24	1.24	—
1000	1.15	1.16	1.10	1.10	1.10	1.10	1.10	—
$(\text{CH}_4 + \text{Cl})/(\text{CD}_4 + \text{Cl})$								
200	45.3	66.3	31.2	25.7	18.1	35.8	35.8	—
250	21.5	29.7	15.8	14.8	10.9	18.6	18.6	—
300	12.8	16.9	9.96	9.17	7.54	11.1	11.1 ^d	12.2 ^e
304	12.4	16.2	9.55	8.90	7.35	10.8	10.8	10.9 ^f
350	8.76	11.1	6.94	6.60	5.66	7.70	7.70	—
400	6.55	7.98	5.30	5.10	4.52	5.79	5.79	5.2 ^f
450	5.21	6.17	4.28	4.15	3.76	4.68	4.68	3.9 ^f
500	4.34	5.01	3.60	3.51	3.24	3.83	3.83	—
1000	1.98	2.07	1.68	1.67	1.64	1.71	1.71	—

^aRef. 3b ^bRef. 5 ^cAn older measurement by Wallington and Hurley (Ref. 4), yielded 1.36 ± 0.04 at 295 K ^dPrevious results from Ref. 14 using analytical potential energy surface at CVT/LCT levels are equal to 41.8, 22.4, 13.9, and 9.56 at temperatures of 300, 350, 400, and 500 K, respectively ^eRef. 6: Single point measurement at room temperature
^fRef. 7

Table 15 Mean unsigned percentage errors in the KIEs calculated at SRP4-IC level.

Method	$^{13}\text{CH}_4 + \text{Cl}$	$\text{CH}_3\text{D} + \text{Cl}$	$\text{CD}_4 + \text{Cl}$
TST	4.4	8.0	19.6
TST/W	3.6	6.8	49.6
CVT	1.4	3.4	12.6
CVT/ZCT	0.4	3.5	51.0
CVT/SCT	1.5	2.7	21.8
CVT/LCT	0.5	8.7	10.4
CVT/ μ OMT	0.5	8.7	10.4

FIGURE CAPTIONS

Figure 1. Transition state structure for the reaction $\text{CH}_4 + \text{Cl}$ (C_{3v} symmetry)

Figure 2. Classical potential energy curve, $V_{MEP}(s)$, and vibrationally adiabatic ground-state potential energy curve , V_a^G , as functions of the reaction coordinate s calculated using rectilinear coordinates by the SRP4[MP2]-IC method.

Figure 3. Value of the breaking bond distance as a function of reaction coordinate in SRP4[MP2]-IC calculation.

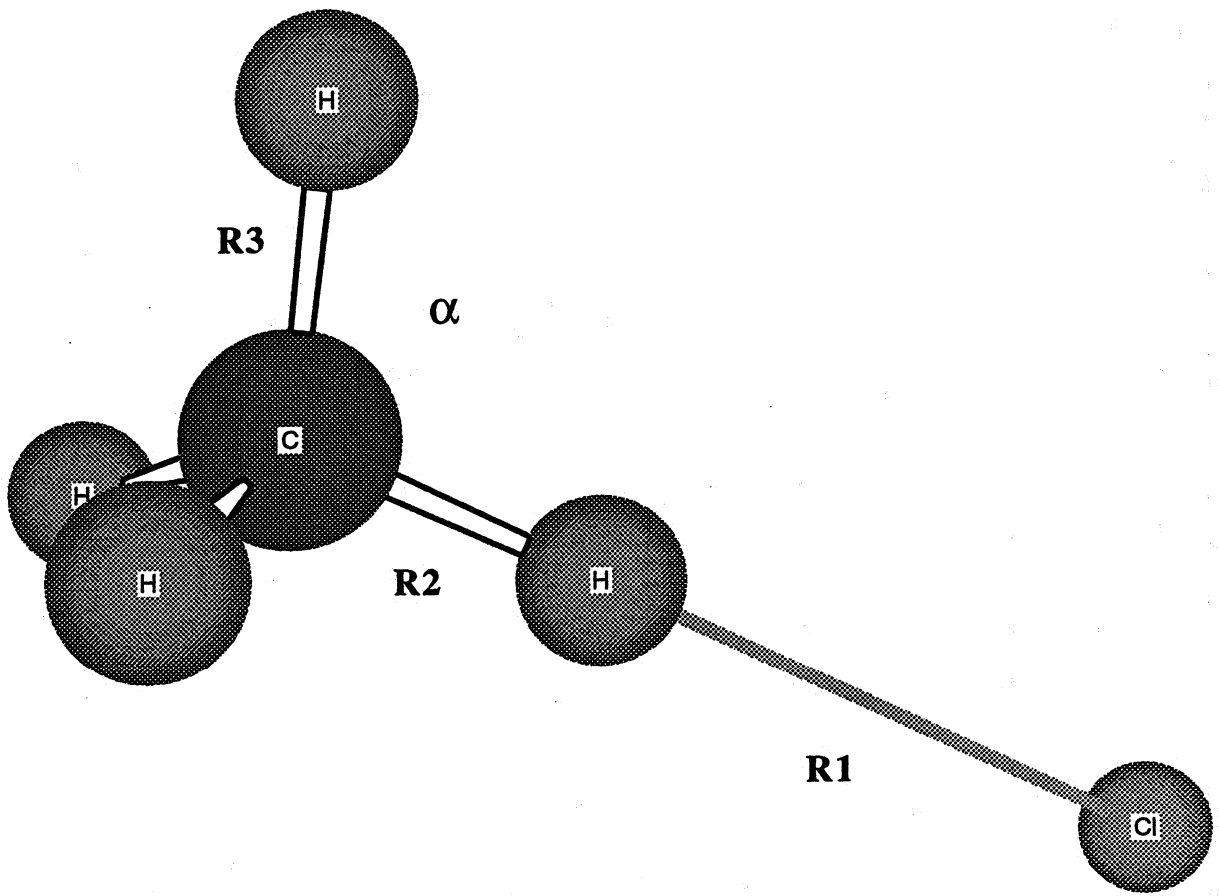


Figure 2

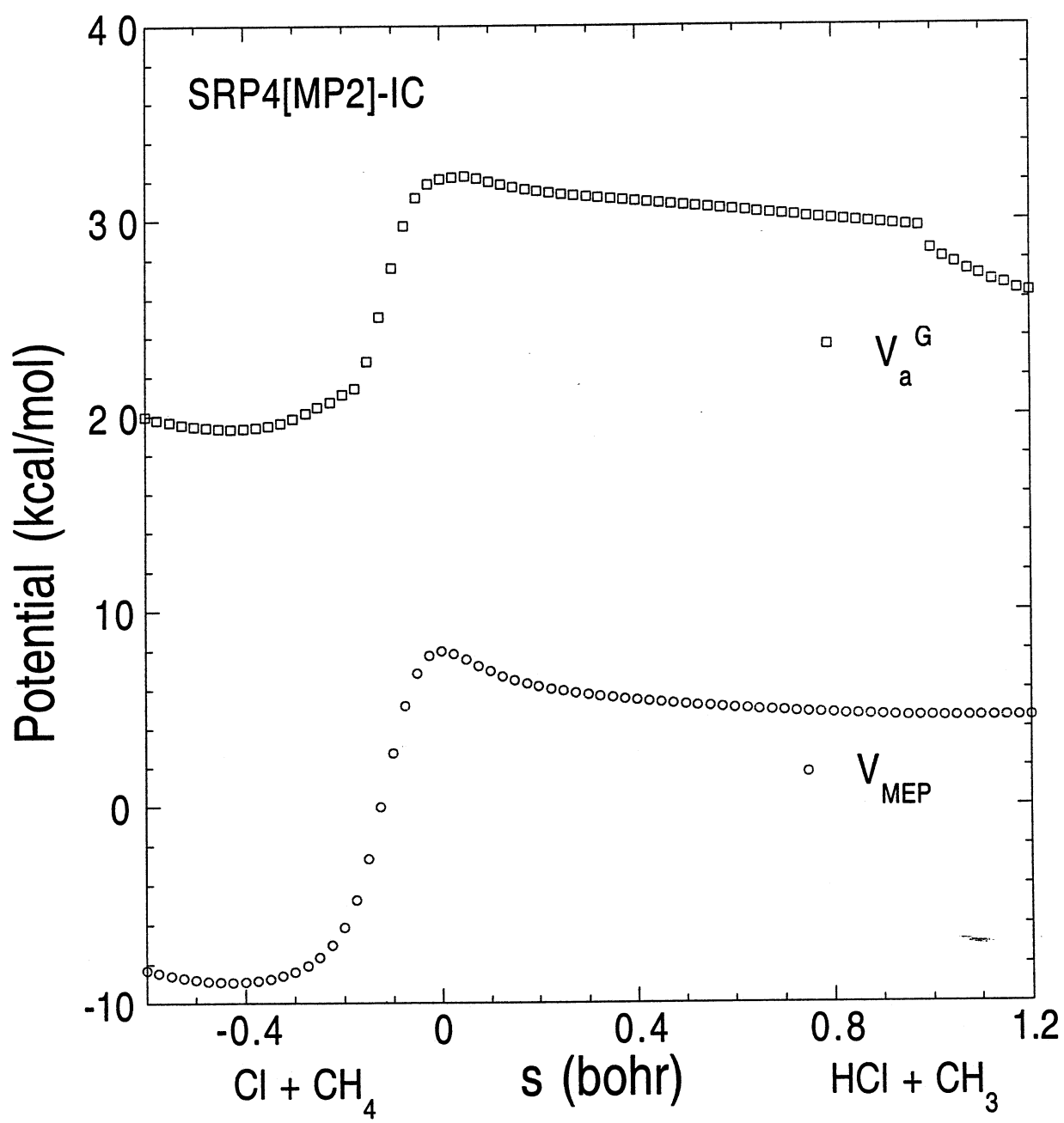


Figure 3

